

# Stability of Antarctic Bottom Water Formation to Freshwater Fluxes and Implications for Global Climate

JESSICA TREVENA, WILLEM P. SIJP, AND MATTHEW H. ENGLAND

*Climate Change Research Centre, University of New South Wales, Sydney, New South Wales, Australia*

(Manuscript received 29 August 2007, in final form 10 December 2007)

## ABSTRACT

The stability of Antarctic Bottom Water (AABW) to freshwater (FW) perturbations is investigated in a coupled climate model of intermediate complexity. It is found that AABW is stable to surface freshwater fluxes greater in volume and rate to those that permanently “shut down” North Atlantic Deep Water (NADW). Although AABW weakens during FW forcing, it fully recovers within 50 yr of termination of FW input. This is due in part to a concurrent deep warming during AABW suppression that acts to eventually destabilize the water column. In addition, the prevailing upwelling of Circumpolar Deep Water and northward Ekman transport across the Antarctic Circumpolar Current, regulated by the subpolar westerly winds, limits the accumulation of FW at high latitudes and provides a mechanism for resalinizing the surface after the FW forcing has ceased. Enhanced sea ice production in the cooler AABW suppressed state also aids in the resalinization of the surface after FW forcing is stopped. Convection then restarts with AABW properties only slightly colder and fresher compared to the unperturbed control climate state. Further experiments with larger FW perturbations and very slow application rates (0.2 Sv/1000 yr) ( $1 \text{ Sv} = 10^6 \text{ m}^3 \text{ s}^{-1}$ ) confirm the lack of multiple steady states of AABW in the model. This contrasts with the North Atlantic, wherein classical hysteresis behavior is obtained with similar forcing. The climate response to reduced AABW production is also investigated. During peak FW forcing, Antarctic surface sea and air temperatures decrease by a maximum of 2.5° and 2.2°C, respectively. This is of a similar magnitude to the corresponding response in the North Atlantic. Although in the final steady state, the AABW experiment returns to the original control climate, whereas the North Atlantic case transitions to a different steady state characterized by substantial regional cooling (up to 6.0°C surface air temperature).

## 1. Introduction

Since Manabe and Stouffer (1988) showed the existence of two different stable ocean circulation states under the same forcing in a global climate model, there have been numerous studies on the stability and variability of the global thermohaline circulation (THC) [see Rahmstorf et al. (2005) and references therein]. The focus of virtually all of these studies has been on the North Atlantic Deep Water (NADW). The maintenance of two stable states of NADW is achieved via salinity feedbacks, as was clearly explained by Bryan (1986). To summarize, there is a thermal preference for high-latitude sinking, but due to the additional dependence of density on salinity, it is possible to generate

positive or negative feedbacks in the system via salt advection. In the North Atlantic case, the salinity feedback is positive. Freshwater (FW) addition over the sinking region will naturally inhibit convection. This results in a slowdown in the rate of flow of high salinity subtropical water to replace the sinking NADW. Thus, there is a positive feedback: If the FW perturbation is applied at a rate strong enough relative to the low-latitude salt input, the original region of freshening becomes rapidly fresher and NADW shuts down.

The shutdown of NADW occurs despite a stabilizing (or negative) thermal feedback that tends to make water residing at the subpolar surface colder and, hence, more dense. When the NADW shutdown persists, the density increase due to this thermal effect is weaker than the density decrease due to surface freshening. This is a finely balanced system: if the initial salt and temperature forcings are different, then there is a different “threshold” for NADW shutdown. The possibility of NADW collapse has sparked a number of studies

---

*Corresponding author address:* Jessica Trevena, Climate Change Research Centre, University of New South Wales, Sydney, NSW 2052, Australia.  
E-mail: j.trevena@unsw.edu.au

on the response of the North Atlantic THC to global warming and/or Arctic sea ice and Greenland ice sheet melting and the effect this would have on climate (e.g., Stouffer and Manabe 2003; Vellinga and Wood 2002; Clark et al. 2002; Yin et al. 2006; Prange et al. 2002).

The Antarctic region's THC is likely to be subjected to enhanced glacial meltwater input over the coming years. However, much less attention has been given to this region's water masses. The processes that maintain the deep THC are fundamentally different between the two hemispheres. In the North Atlantic, surface salt flows northward in the western boundary current of the North Atlantic subtropical gyre, resulting in the positive and negative feedback loops discussed above. In the Antarctic oceans, by contrast, any geostrophic connection is "blocked" by the Drake Passage gap where there is no "western boundary" to permit geostrophically balanced flow. Surface meridional flow is northward via ageostrophic Ekman transport at the latitudes of the Drake Passage gap, and the balancing deep return flow can only occur at depths where the presence of deep ocean ridges allows the north/south flow to be geostrophically balanced (Toggweiler and Samuels 1995). Thus, the interaction between subpolar waters and subtropical saline waters does not occur directly via the subtropical gyres in the Southern Hemisphere. It is instead upwelled deep water that brings salt to the high latitudes of the Southern Hemisphere oceans, made up largely of outflowing NADW that is converted into Circumpolar Deep Water (CDW) (Goodman 1998; Orsi et al. 2001). The westerly winds control this upwelling of higher salinity CDW (Toggweiler and Samuels 1993), a process which Goodman (1998) notes is despite most of the global positive buoyancy forcing occurring farther north between 30°S and 30°N. Once at the surface, strong heat loss to the atmosphere along with brine rejection during sea ice formation transforms a significant portion of the upwelled water to higher densities, and it sinks along the Antarctic continental shelf, contributing to the bottom-ventilating water mass of the Southern Hemisphere Antarctic Bottom Water (AABW). The importance of the westerly winds in maintaining this process was demonstrated by Toggweiler et al. (2006), who showed that a decrease in magnitude of the Southern Hemisphere westerly winds significantly reduced AABW formation rates (also noted by Rahmstorf and England 1997; Saenko et al. 2002). Toggweiler et al. also postulate that a northward shift of the winds would have a similar effect via less upwelling of saline CDW and because the upwelling of CDW would occur at lower, warmer latitudes where transformation to dense AABW through heat loss to the atmosphere is less easily facilitated. This has recently been

confirmed in a series of equatorward wind shift experiments by Sijp and England (2008, manuscript submitted to *J. Phys. Oceanogr.*). Another major difference between the Southern and Northern Hemispheres is the thermal isolation of Antarctica. This contributes to the formation of extensive areas of sea ice over AABW formation regions, which injects salty brine into the surface ocean, helping to maintain high surface densities and localized deep convective overturn (Orsi et al. 1999) despite a largely stable halocline environment of the polar ocean (Keeling and Stephens 2001).

The existence of multiple equilibria in the ocean's thermohaline circulation depends on a few critical ingredients. First, the aforementioned "positive" (salinity) and "negative" (temperature) feedbacks need to act in competition at the region of water mass formation. Second, in terms of salinity, the internal horizontal oceanic FW fluxes into the region of water mass formation must be of opposite sign to the combined air-sea and ice-sea fluxes acting across the sea surface (e.g., Rahmstorf 1996). This is required so that any collapse of the ocean overturning circulation is not reinvigorated by the buoyancy loss arising from both thermal and haline surface forcing. The above conditions are clearly met in the North Atlantic, wherein the northward advective salt fluxes act to oppose the prevailing surface freshening over the region's deep-water formation regions (the latter comes about via an excess of precipitation over evaporation). In contrast, with at least three regions of bottom water formation around the Antarctic continental margin and limited direct observations of the surface ocean freshwater fluxes, it remains unclear whether multiple equilibria are possible for AABW. One of the main goals of the present study is to assess the possibility of multiple equilibria in the high-latitude Southern Ocean THC.

There have been limited studies of the stability and variability of AABW production to imposed climate change. Bi et al. (2001) examined the response of AABW to increasing atmospheric CO<sub>2</sub>, finding that the surface ocean warming and enhanced hydrological cycle lead to a cessation of AABW production. However, once warming penetrates the deep ocean (in this case, after around 900 yr), vertical density gradients return close to control conditions and convection and AABW formation is reestablished. Bates et al. (2005) also examined the Southern Hemisphere response to atmospheric CO<sub>2</sub> increase, finding that the Antarctic Circumpolar Current (ACC) strengthens and, while AABW production initially decreases, it eventually recovers and actually increases, from 12 Sv to 16 Sv (1 Sv = 10<sup>6</sup> m<sup>3</sup> s<sup>-1</sup>). Brix and Gerdes (2003) examined the

response of AABW to positive and negative salinity anomalies of 1 psu over the Weddell Sea, finding that AABW production naturally intensifies in the positive anomaly case and weakens in the negative anomaly experiment. Interestingly, the negative salinity anomalies were observed to have a smaller influence on Antarctic and global overturning; although notably Brix and Gerdes (2003) used restoring boundary conditions, which inhibit the ocean–atmosphere and ocean–ice feedbacks that might have otherwise affected the response.

In contrast to the above studies, the goal here is to examine the stability of AABW in a preindustrial climate using a global model that internally predicts surface ocean freshwater fluxes. The response of AABW to varying FW perturbations will be examined in a global intermediate complexity climate model. This differs from most previous studies that have considered the AABW response to increased greenhouse gases, surface warming, imposed surface salinity changes, and westerly wind strength changes. We do not include an interactive carbon cycle, as we wish to investigate the effects of temperature and salinity feedbacks on the Southern Hemisphere THC in isolation from carbon feedbacks. We explain the results in terms of the different salinity feedbacks operating in the global ocean and demonstrate that in the current climate model configuration, an AABW “off” state is unstable. We also quantify the climate response to a transient slowdown in the AABW THC.

The rest of this paper is divided as follows: section 2 outlines the model and experimental design, while section 3 analyzes the results, with an emphasis on the difference between the Antarctic and North Atlantic response to FW perturbations. Section 3 also includes the results of hysteresis experiments and the analysis of the climate response to FW perturbations. Finally, section 4 covers a summary and conclusions of the main findings of the study.

## 2. Climate model and experimental design

### a. Climate model

We use the University of Victoria Intermediate Complexity Climate (UVic) model (Weaver et al. 2001), suitable for multimillennial simulations of the global climate system. The ocean model component has 19 depth levels, a resolution of  $1.8^\circ$  latitude  $\times$   $3.6^\circ$  longitude, and is coupled to a simple energy–moisture balance model of the atmosphere and a dynamic–thermodynamic model for sea ice. The atmospheric model includes advection and diffusion of moisture, which has been shown to improve the global salinity distribution

(Weaver et al. 2001). The sea ice model includes prediction of the ice thickness and ice area fraction in each grid cell, though it is only a single category sea ice model. The brine beneath sea ice is convected according to the parameterization of Duffy and Caldeira (1997). Recently, a more realistic multicategory sea ice model (Bitz and Lipscomb 1999) has been incorporated into the UVic model, though we found no significant differences in the results using this newer multicategory sea ice model. The climate model is linked to a prescribed Antarctic land–ice sheet that is static in time. Shelf mixing processes, whereby dense, saline surface water sinks to the Antarctic continental shelf and then overflows via density plumes into the deep ocean, are not resolved explicitly in the model. This is a common feature of global climate models suitable for multimillennial integrations. Such shelf processes depend on high-resolution ocean physics and bottom bathymetry, which can only be parameterized in large-scale models. However, our focus is not on quantifying the variability of AABW, but on developing an understanding of basic salt feedback processes operating in the Antarctic and Southern Ocean regions at large scales.

Vertical diffusion varies according to the depth profile of Bryan and Lewis (1979), ranging from  $0.3 \text{ cm}^2 \text{ s}^{-1}$  beneath the surface mixed layer to  $1.3 \text{ cm}^2 \text{ s}^{-1}$  at the ocean bottom. The thickness of the surface ocean layer is 50 m, increasing to 500 m at the ocean abyss. Enhanced wind-driven surface mixing is approximated using a vertical diffusion coefficient of 1 and  $0.5 \text{ cm}^2 \text{ s}^{-1}$  in the top two layers. In addition, the ocean model incorporates the Gent and McWilliams (1990) parameterization of eddy advection effects, implemented by way of an advection velocity acting on the tracer fields. We use identical isopycnal and isopycnal thickness diffusion coefficients of  $4 \times 10^6 \text{ cm}^2 \text{ s}^{-1}$ , with a maximum isopycnal slope of 1 in 100. Although the isopycnal diffusion coefficients are quite low, experiments with higher coefficients of  $2 \times 10^7 \text{ cm}^2 \text{ s}^{-1}$  showed no appreciable differences. It is known that vertical mixing is also important in determining deep overturning rates and their stability (see, e.g., Sijp and England 2006). In this study, we only consider different Gent and McWilliams (1990) strengths, leaving a detailed sensitivity study of vertical diffusion to another study. The horizontal diffusion coefficient is set to zero throughout the global ocean. We use a constant lateral mixing coefficient for momentum of  $2 \times 10^9 \text{ cm}^2 \text{ s}^{-1}$ , while the constant vertical mixing coefficient for momentum is  $10 \text{ cm}^2 \text{ s}^{-1}$ . The release of potential energy by convective overturning of the water column is modeled using the convective adjustment algorithm described by Rahmstorf (1993; see also Pacanowski 1995). A rigid-lid ap-

proximation is used and surface FW fluxes are modeled by way of an equivalent salt flux calculated using a fixed reference salinity.

The model is forced with present-day insolation, pre-industrial CO<sub>2</sub> of 280 ppm, and present-day land-ice. Air and ocean temperatures, as well as ocean salinity, are allowed to evolve freely. Wind is fixed within an annual cycle based on the monthly fields from the National Centers for Environmental Prediction–National Center for Atmospheric Research (NCEP–NCAR) re-analysis over the period 1958–97 (Kalnay et al. 1996), though to confirm the validity of our results further experiments with wind feedbacks were also conducted. In the case of no wind feedback, the westerly winds overlying the ACC are unable to respond to changes in local sea surface temperatures, although it has recently been demonstrated that this feedback is weak (Sen Gupta and England 2007).

The equilibrium control (CNTRL) state obtained with the above specifications generates approximately 21.0 Sv of NADW. Formation of AABW is characterized by a cell of strength 3.5 Sv, corresponding to overturning adjacent to Antarctica (Fig. 2 inset). This apparently weak AABW overturning is, however, based on a zonal integral of vertical transport that averages out downwelling and upwelling fluxes. When downwelling and upwelling are considered separately to remove zonal aliasing, they amount to a net 11.4 Sv downwelling and 7.9 Sv upwelling south of 67°S at a depth of 1000 m (giving the net overturning maximum of 3.5 Sv). Deeper, at 2500 m, the net downwelling south of this latitude is 5.1 Sv; this increases if we include latitudes farther north to 63°S. The model's AABW formation, measured in terms of net downwelling, is in reasonable agreement with the 8.1 Sv of AABW production determined by Orsi et al. (2001) using a chlorofluorocarbon-11 budget analysis. Another measure of the model's AABW strength, which depends less on aliasing, is the net northward flow of bottom water in the abyssal cell centered near 40°S (Fig. 2 inset). This cell has a strength of 11.7 Sv in the CNTRL climate state, a similar strength to that seen in the Commonwealth Scientific and Industrial Research Organisation (CSIRO) model used by Bi et al. (2001, their Fig. 1a), and falls well within the range of model- and observation-based estimates of 4 Sv (Brix and Gerdes 2003) and 27 Sv (Talley et al. 2003).

A comparison of the zonal-mean water properties in the CNTRL case with climatological (Levitus et al. 1994; Levitus and Boyer 1994) annual mean temperature and salinity fields shows that the model's AABW is slightly too fresh and cold, but within reasonable agreement of the observed. Globally averaged tem-

perature and salinity ( $T$ – $S$ ) over the bottom layer of the ocean model are 0.77°C and 34.70 psu compared to the 0.91°C and 34.73 psu observed. The overall model  $T$ – $S$  structure agrees well with the observed (Fig. 1) and is comparable to the Intergovernmental Panel on Climate Change (IPCC) class ocean climate models (see, e.g., Griffies et al. 2008, manuscript submitted to *Ocean Modell.*). Apparent in the zonal mean is a tongue of low-salinity Antarctic Intermediate Water (AAIW) extending to depths greater than 1000 m in the midlatitudes of the Southern Hemisphere. This overlays warm saline NADW in the Atlantic basin while abyssal cold and fresher AABW is found in the deepest layers of the Atlantic, Pacific, and Indian Ocean abyss.

The model's zonally integrated meridional salt transport (figure not shown) indicates that, like the North Atlantic Ocean, the internal oceanic advective salt fluxes are poleward into the AABW formation regions. Thus, as described in section 1, one necessary condition for the existence of multiple equilibria for AABW is satisfied. Concerning the other necessary condition, namely, net FW gain via air–sea and ice–sea fluxes, the net surface fluxes are, for the most part, adding FW to the AABW formation regions, apart from a localized band of FW loss due to sea ice formation along the highest latitude row of model grid points (figure not shown). Thus, it is unclear that the second condition for multiple equilibria of AABW in the model will be met. This will be explored further in section 3.

### b. Experimental design

We apply a positive FW flux to the ocean surface south of 63°S (experiment FW<sub>SO</sub>) that increases linearly at a rate of 0.004 m yr<sup>-2</sup> (see Fig. 2 lower panel). This area encompasses the Ross and Weddell Seas, as well as almost the entire region where surface ocean potential temperature is less than -0.5°C, the upper limit taken for many AABW studies (see, e.g., Orsi et al. 1999). The pulse is triangular in time, 300 yr in length, and increases to a maximum value of 0.26 Sv at year 150, which is commonly above the threshold for NADW shutdown (e.g., Rahmstorf et al. 2005). Even pulses 5 times this size produced qualitatively similar results to those presented below. For the corresponding North Atlantic experiment (FW<sub>NA</sub>), we apply the FW flux between 52° and 75°N over the Atlantic. The length of the pulse and volume of water applied in the FW<sub>NA</sub> experiment are identical to those in FW<sub>SO</sub>, though the areas differ (FW<sub>SO</sub> covers approximately twice the area compared to FW<sub>NA</sub>). We also repeated the FW<sub>SO</sub> experiment with much larger FW pulses (up to a peak of 2 Sv) and obtained robust results to those presented below.

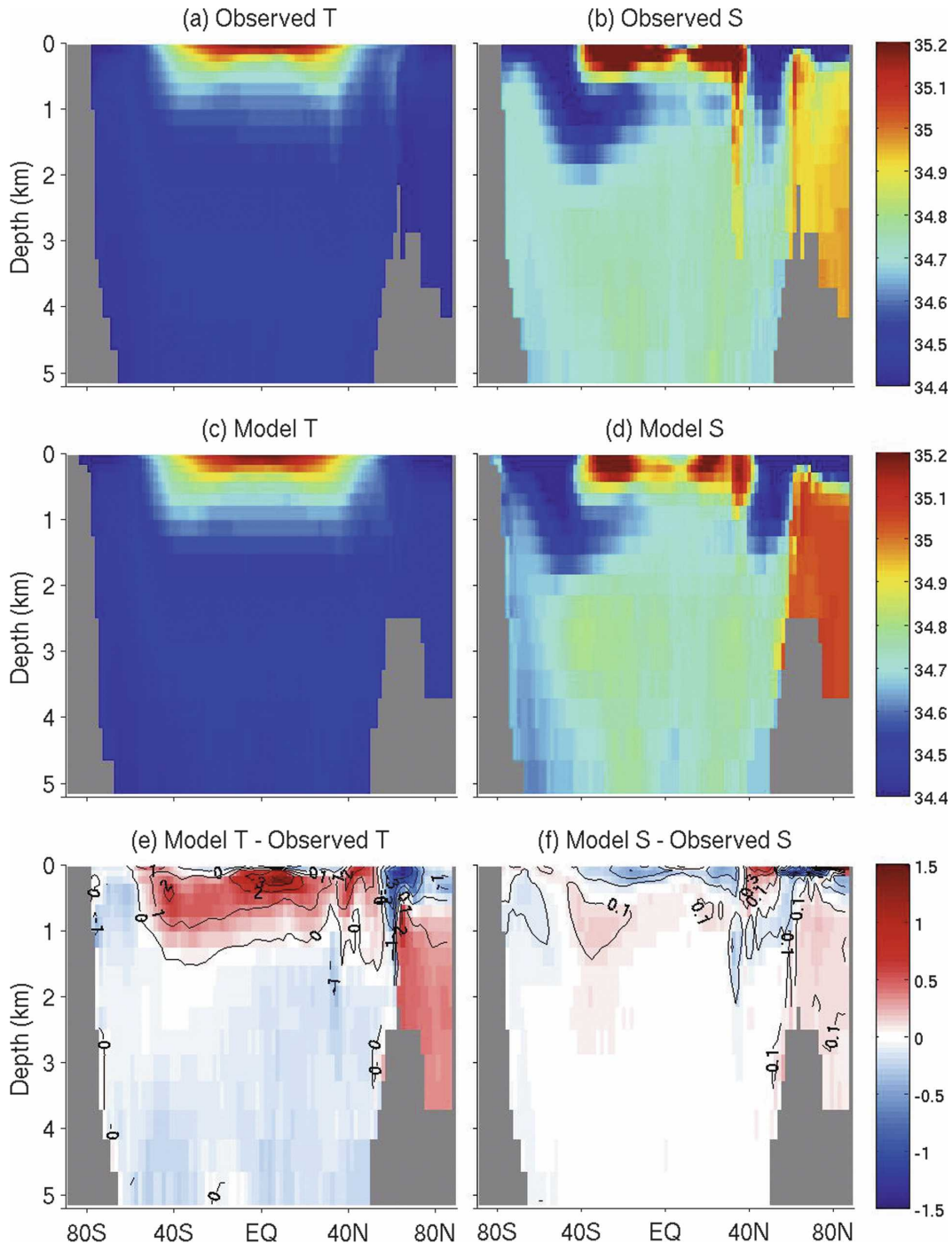


FIG. 1. (top) Observed temperature and salinity from Levitus et al. (1994) and Levitus and Boyer (1994), and (middle) model temperature and salinity for the the CNTRL steady state. (bottom) Anomaly (model–observed) for temperature ( $^{\circ}\text{C}$ ) and salinity (psu).

### 3. Results

#### a. Meridional overturning circulation

Figure 2 shows the time series of AABW and NADW in response to the FW pulse additions in  $\text{FW}_{\text{SO}}$

and  $\text{FW}_{\text{NA}}$ . For NADW, the measure is the maximum in the Atlantic sector meridional overturning streamfunction (see Fig. 3b) north of  $33^{\circ}\text{N}$ . For AABW, there are two time series. The first is the minimum in the streamfunction between  $63^{\circ}\text{S}$  and Antarctica and be-

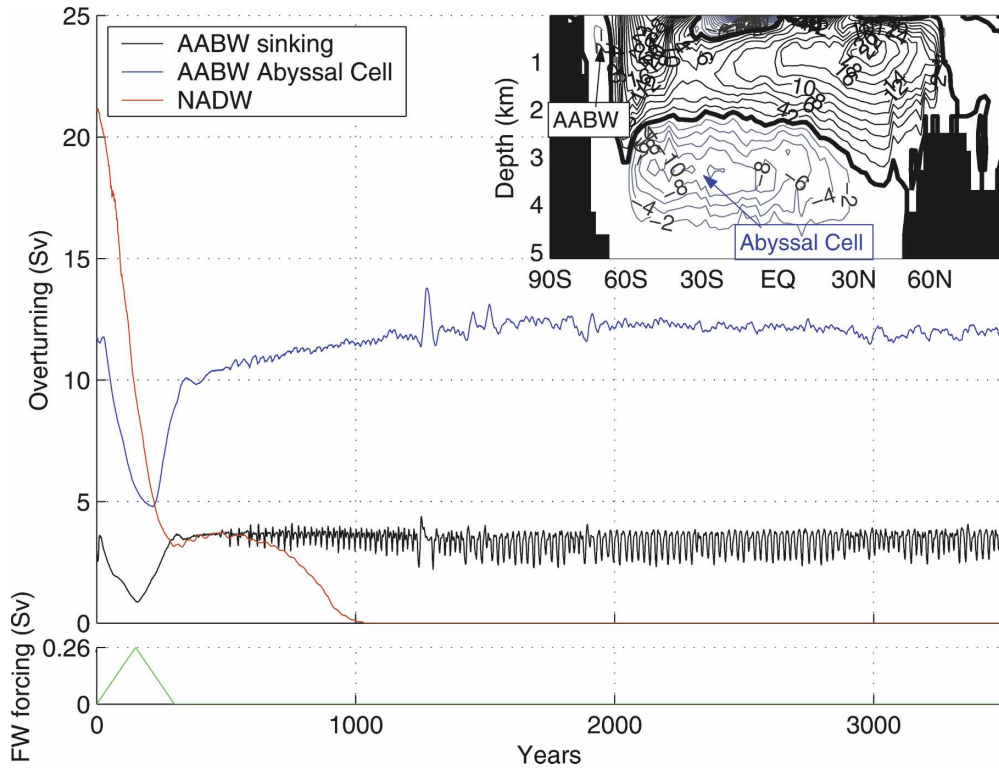


FIG. 2. Overturning time series response to a 300-yr symmetrical FW pulse, reaching a maximum rate of 0.26 Sv. Black curve indicates the zonally integrated AABW overturning adjacent to Antarctica; blue curve is the abyssal cell centered near 30°–40°S; and the red curve is NADW overturning. The AABW curve is for expt  $FW_{SO}$  and the NADW is for expt  $FW_{NA}$ . Also shown in the inset is the initial condition (CNTRL) meridional overturning circulation (MOC) showing the location of the AABW cells plotted in the time series.

tween 177 and 2497 m depth. The second is the bottom water outflow south of 33°S and below 2500 m, otherwise known as the “abyssal cell” owing to its equivalence to the maximum zonally integrated northward transport of bottom water. The location of both these cells is indicated in the inset of Fig. 2.

During the period of the FW pulse in  $FW_{NA}$ , NADW decreases rapidly (Fig. 2, red line) before showing what appears to be the beginning of a recovery after the FW addition period ends. The NADW cell then decreases again to reach zero by year 1000, when it remains stable for thousands of years. Thus, the North Atlantic overturning switches to a stable “off” state in experiment  $FW_{NA}$ . The overturning cell seen in the Northern Hemisphere in Fig. 3g corresponds to overturning in the North Pacific, which develops when NADW is suppressed, consistent with the work of Saenko et al. (2004). In contrast, in experiment  $FW_{SO}$  the AABW sinking cell decreases to nearly zero (0.9 Sv) during the period of the pulse but recovers within only 30 yr after the FW flux ends, reaching a quasi-steady-state value of 3.5 Sv. Although this appears to be a decrease of only

75%, it should be remembered that this value is a measure of the minimum in the overturning streamfunction south of 63°S, which also shoals significantly during the pulse period, from 1000 to 200 m (Figs. 3a,c). When upwelling and downwelling are considered as a function of depth (see below), net downwelling decreases to zero in all but the top 200 m of the water column, showing that bottom-water formation has essentially decreased to zero. The abyssal cell also reduces during the period of the FW pulse, decreasing from 11.7 Sv to 4.8 Sv, only to recover back to just over 10 Sv by year 350 and to its control state value of 11.7 Sv by year 1000. After year 1000, the bottom-water cell gradually increases to remain quasi stable just above the control state at 12.0 Sv. The AABW sinking adjacent to Antarctica responds to the FW forcing within a decade or two, while the abyssal cell has a maximum response about 80 yr after the maxima in the FW pulse. Given that the deep ocean typically responds on longer time scales than the more rapidly ventilated near-surface layers, this is not surprising.

A third measure of AABW is obtained by decom-

posing the net upwelling and downwelling adjacent to Antarctica (figure not shown), bearing in mind that the meridional overturning streamfunction is a zonal integral that aliases vertical motion. Though upwelling and downwelling decrease during the FW pulse period, downwelling decreases more, decreasing from 11.4 Sv to 2.9 Sv at 1000 m, while upwelling decreases only from 7.9 Sv to 3.7 Sv at the same depth. Thus, by any measure AABW production slows in response to FW addition, but only temporarily before recovery to its pre-perturbation values. During  $FW_{SO}$ , NADW increases by 1.5 Sv during the period of the pulse owing to increased density contrasts between the Southern Ocean and the North Atlantic, which promote increased NADW production (Saenko et al. 2003). After the pulse, NADW returns to its equilibrium value of 21.0 Sv. During  $FW_{NA}$ , AABW sinking decreases by less than 0.5 Sv. It appears that this is due to a reduction in the salinity of upwelled CDW in the Southern Ocean, though further studies are needed to confirm this. The abyssal cell strength shows an initial decrease of around 1.0 Sv during the period of NADW shutdown before returning to close to its initial value a few centuries after NADW formation has reached zero. It should be noted that the AABW–NADW interaction is limited due to a deep Drake Passage in the present-day climate (see Sijp and England 2005).

The final state meridional overturning streamfunctions for CNTRL,  $FW_{NA}$ , and  $FW_{SO}$ , as well as for  $FW_{SO}$  at 150 yr (the time of maximum AABW sinking response) are shown in Fig. 3. During the period of the Southern Ocean FW pulse, AABW net sinking is almost entirely suppressed and the deep outflow from the North Atlantic deepens and strengthens. The strengthening and deepening are associated with an increase in NADW overturning (1.7 Sv) and export into the Southern Ocean (1.8 Sv) while AABW is suppressed. This increase in NADW can be explained by increased surface Ekman transport of freshwater (originating from the imposed FW anomaly south of the ACC), where it causes AAIW to become fresher, less dense, and hence favor increased NADW sinking (see also Saenko et al. 2003). NADW now fills, at least temporarily, more space in the abyss with the densest, bottommost water mass in the World Ocean (AABW) suppressed.

The final state meridional overturning streamfunctions in Fig. 3 show that the global and Atlantic overturning after 4000 yr in  $FW_{NA}$  is significantly different from CNTRL, with a permanently collapsed NADW cell. On the other hand,  $FW_{SO}$  at 4000 yr shows a state almost identical to CNTRL. The only noticeable difference between  $FW_{SO}$  at 4000 yr and CNTRL is a very slight northward extension of the AABW overturning

adjacent to Antarctica and a slightly deeper penetration of this cell. We hypothesize that this small departure of the final steady state from CNTRL is due to additional FW now in the system. A lower salinity ocean leads to less stratification and thus deeper convection under the same surface forcing.

#### b. Water mass properties

Zonal mean differences in  $T$ – $S$  and a passive tracer for NADW are shown in Fig. 4 at the height of the FW pulse (150 yr) in experiments  $FW_{NA}$  and  $FW_{SO}$ . The passive tracer is applied with concentration unity at each time step to the ocean surface between 48°S and 66°N. If and when the water returns to the surface outside this domain, its concentration is reset to zero. When NADW is suppressed in  $FW_{NA}$ , the deep North Atlantic becomes cumulatively fresher due to a lack of salty water sinking (Keeling and Stephens 2001), and salt accumulates in the surface ocean of the midlatitudes (Fig. 4b). The salinity decrease in the North Atlantic above 1500 m has a maximum zonal average value of 0.28 psu, while the zonal mean salinity increase at the surface midlatitudes is up to 0.27 psu. The deep North Atlantic also cools during NADW suppression, by a maximum of 4.1°C (Fig. 4d), owing to a lack of NADW sinking and more ventilation now occurring via cold Southern Hemisphere water. The near surface midlatitude Atlantic warms by 1.5°C (Fig. 4d), with less tropical warm water pumped northward to replace sinking NADW. Stratification induced by the surface freshening in the North Atlantic leads to further freshening and stratification (via processes discussed in section 1), which then leads to further suppression of NADW overturn, cooling the deep ocean further. Cooler Labrador Sea surface waters (up to 3.8°C) are subducted, contributing to the cooling seen in the shallow layers of the North Atlantic. A passive dye tracer injected into the North Atlantic surface shows a maximum zonal average decrease above 1500 m of 25% already by year 150 (Fig. 4f), indicating the rapid decrease in production of this water mass in experiment  $FW_{NA}$ . The increase in this tracer seen further south is due to less southward transport of NADW (not shown).

When AABW is suppressed in  $FW_{SO}$ , the deep and bottom water  $T$ – $S$  both increase, as shown in Figs. 4a,c, and the surface Southern Ocean cools. Elsewhere the ocean is little affected. Maximum zonally averaged deep  $T$ – $S$  differences (from CNTRL) between 500- and 2500-m depth are approximately 1.4°C and 0.09 psu. The zonal mean surface cooling and freshening is up to –1.3°C and –1.1 psu. Both the deep  $T$ – $S$  increase and the surface  $T$ – $S$  decrease can be explained by less over-

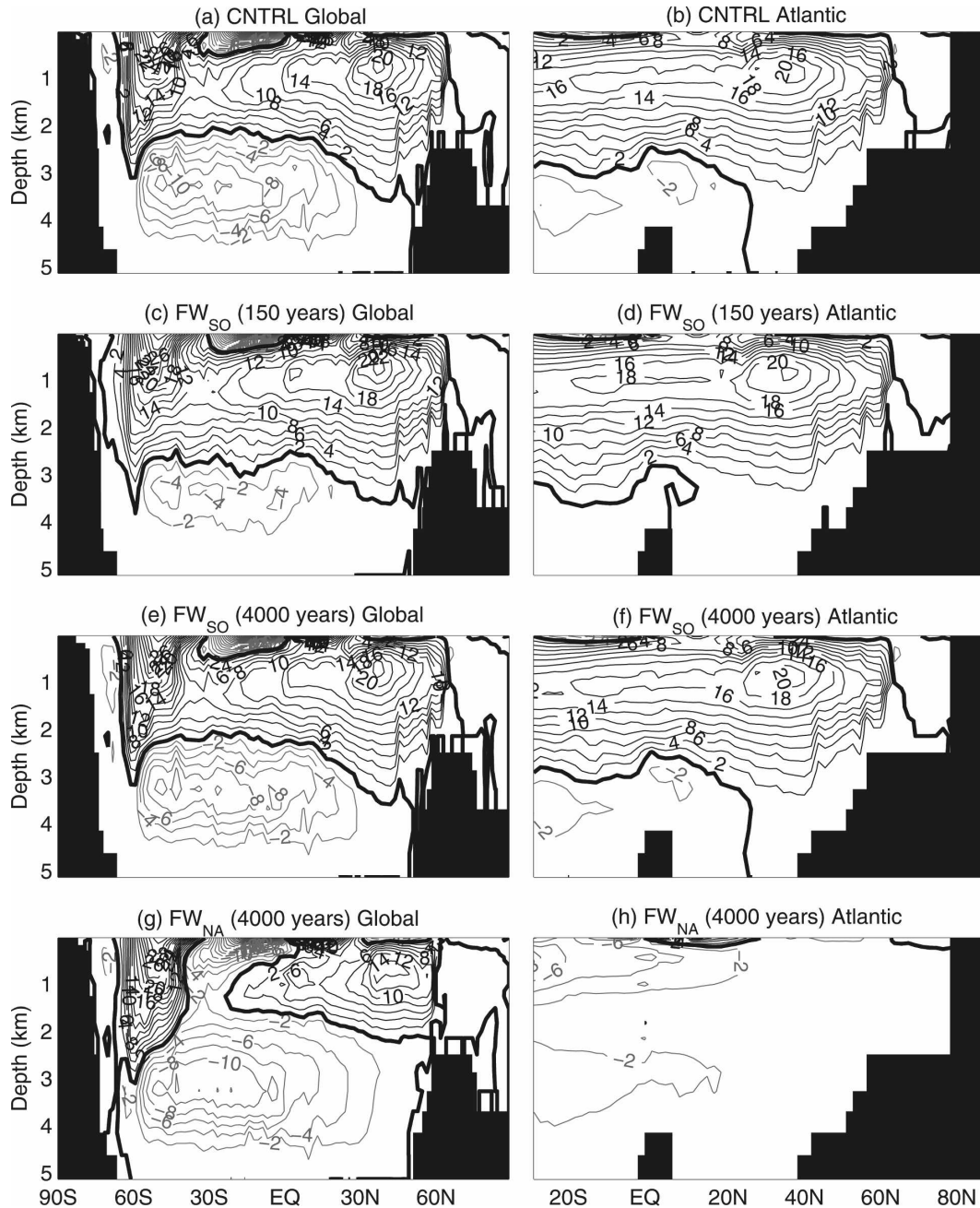


FIG. 3. Final steady-state meridional overturning circulation for expts CNTRL,  $FW_{SO}$ , and  $FW_{NA}$  for the (left) global ocean and (right) Atlantic Ocean. Also shown is the MOC in  $FW_{SO}$  at the time of maximum AABW sinking response (150 yr). Values (Sv) are based on a 1-yr average.

turning of cold, fresh AABW into the interior. Suppressed convection over the AABW formation regions leads to less warm water being drawn upward to replace the sinking water, forcing the deep ocean to warm and the surface ocean to cool. This upwelling of warmer water provides a fundamental limit to sea ice growth in the current Antarctic climate system (Goodman 1998).

Hence, in the suppressed state where this upwelling is significantly reduced, sea ice grows compared to CNTRL (Fig. 5a). Suppressed overturning of surface waters also prevents natural FW input, such as precipitation and summer meltwater, from mixing into the interior, thus further increasing the deep ocean salinity. The  $T-S$  changes in the deep ocean are also influenced

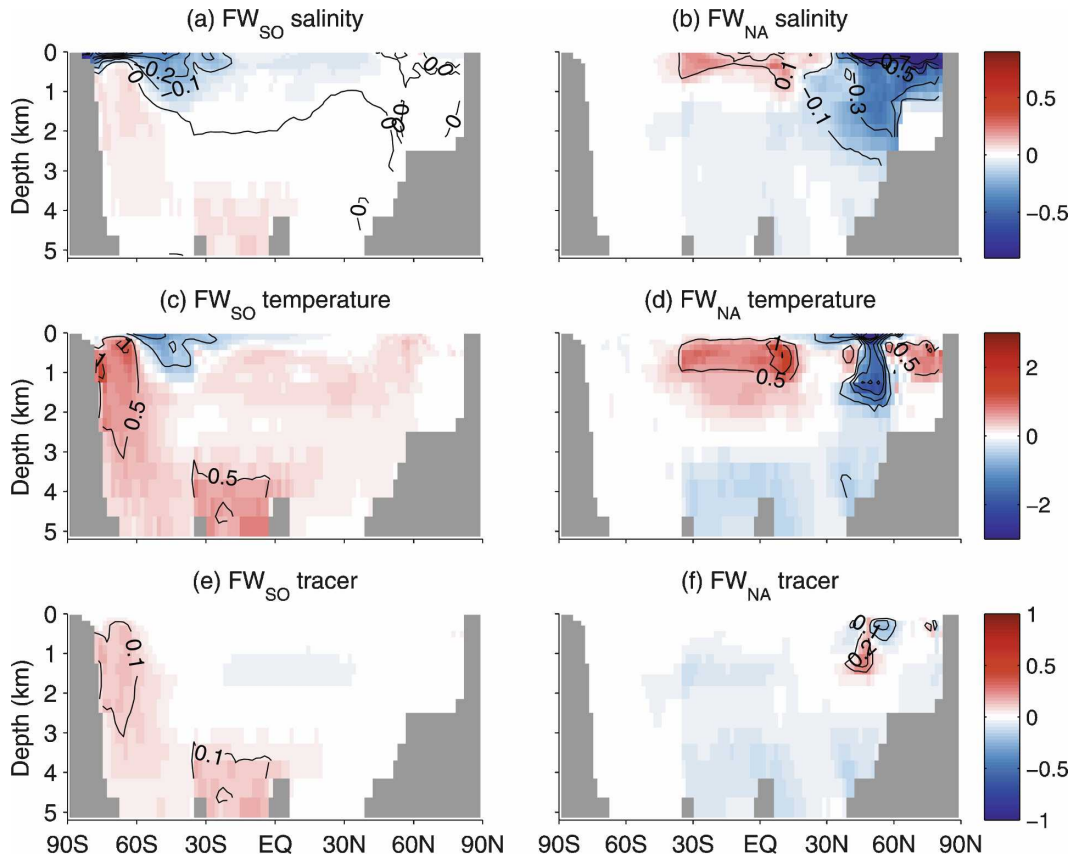


FIG. 4. Zonally averaged difference fields (from CNTRL) for salinity (psu), temperature ( $^{\circ}\text{C}$ ), and a passive NADW tracer (fraction of tracer) for (left)  $\text{FW}_{\text{SO}}$  and (right)  $\text{FW}_{\text{NA}}$ . The zonal mean includes the Atlantic basin plus a circumpolar average in the Southern Hemisphere south of  $36.9^{\circ}\text{S}$ . The data are averaged for 1 yr at the height of the FW pulse (150 yr). Note that the scale for each parameter is the same between experiments.

by the increase in deep southward transport of warm saline NADW from the Northern Hemisphere (seen in Figs. 3c,d). This warm, saline water is transported southward across the ACC and upwelled around Antarctica, increasing the volume of relatively warm, saline water in the deep Antarctic Ocean and reinforcing the  $T$ - $S$  changes seen there.

While AABW is temporarily suppressed in  $\text{FW}_{\text{SO}}$ , more of the ocean's deep and bottom water is sourced from the North Atlantic at the expense of the Antarctic source regions. This is confirmed in an analysis of the difference in concentration of a North Atlantic passive tracer at 150 yr between  $\text{FW}_{\text{SO}}$  and CNTRL (Fig. 4e). At depths greater than a few hundred meters, the passive tracer shows a maximum zonal average increase of up to 18% already by year 150. This increase is due to an increase in NADW sinking and production, which is then transported into the ACC to constitute CDW, and a reduction in the amount of AABW overturned locally within the Southern Ocean. Both of these effects act to

increase the volume of saline NADW in the deep and abyssal ocean south of the ACC.

The deep warming in  $\text{FW}_{\text{SO}}$  reduces the stability of the water column, while the deep salinity increase tends to stabilize it. Relative to CNTRL, increased surface salinity fluxes from sea ice and steady vertical ocean salt transport (CDW upwelling) during AABW suppression (Fig. 5b) weaken the stability of the water column by the end of the FW pulse (seen later in Fig. 7a). Indeed Fig. 6b, which will be discussed in more detail in section 3a, shows that soon after the FW forcing has ceased, surface salinities increase above that of CNTRL and convection and overturning restart, as seen in Fig. 2.

Closer examination of Fig. 2 shows that the overturning response follows soon after the changes in the FW pulse, indicating a nearby salt source that prevents FW accumulation in the area around Antarctica. In the current climate, the accumulation of FW from high precipitation rates over the Southern Ocean is prevented by efficient northward Ekman transport of the surface

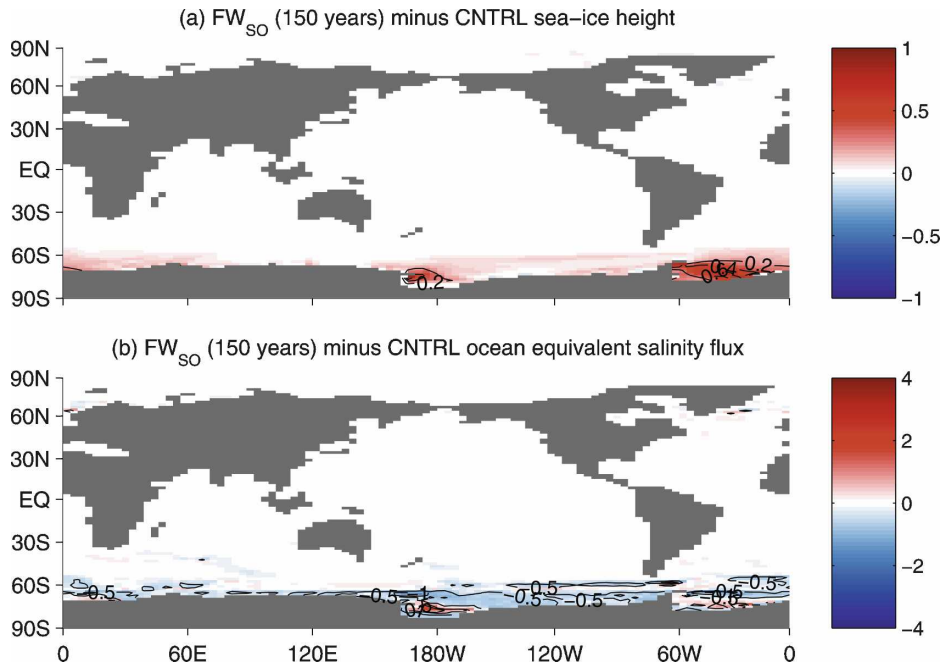


FIG. 5. Difference in (a) sea ice height (m) (interval: 0.2 m) and (b) equivalent surface salt fluxes ( $\text{kg m}^{-2} \text{s}^{-1}$ ) (interval:  $0.5 \text{ kg m}^{-2} \text{s}^{-1}$ ) for  $FW_{SO}$  at 150 yr (difference from CNTRL). The equivalent ocean salt flux term includes  $E-P$  and sea ice fluxes, but not the FW perturbation added to the Antarctic Oceans. Positive values indicate increased sea ice height and net salt flux into the ocean. All fields are based on a 1-yr average.

FW (in the form of both water and sea ice). This transport constitutes a net positive salt flux over AABW formation regions, important for AABW maintenance (Saenko and Weaver 2001; Orsi et al. 1999). In addition to the northward Ekman transport, positive salt fluxes from the upwelling of saline CDW are also known to be important for maintaining AABW formation (Goodman 1998; Toggweiler et al. 2006). The combination of upwelling saline CDW, together with the northward Ekman transport of FW, can be seen as a “flushing” mechanism for the high-latitude Southern Ocean, whereby salt is constantly returned and FW constantly removed (see the schematic in Fig. 6a). Most importantly, these two processes persist during the period of FW perturbation, in distinct contrast to the North Atlantic, wherein a FW addition can collapse the poleward salt transport replenishment process. This fundamental difference between the Antarctic and North Atlantic Oceans provides an explanation for the observed stability of AABW seen in the model.

### c. Mechanisms removing the Southern Ocean FW anomaly

It is argued above that the upwelling of CDW provides a constant source of salinity to the high-latitude

Southern Ocean that persists regardless of FW perturbations. With winds fixed in the model, this is easy to demonstrate as the equation for wind-driven upwelling:

$$w = \frac{\nabla \times \tau}{f\rho} \quad (1)$$

(where  $\tau$  is horizontal wind stress,  $f$  the Coriolis parameter, and  $\rho$  ocean water density) shows a negligible dependence on ocean density, as  $\rho$  appears in the denominator. We have made the approximation that  $f$  is constant, which is commonly done (Gill 1982) since the Coriolis force varies more slowly than wind stress in the region of Drake Passage. In the real system, FW anomalies could trigger circulation changes that feed back to alter the wind field, thus affecting CDW upwelling as per Eq. (1). To assess this, similar experiments are conducted in which a wind feedback is employed. In such experiments, Ekman pumping changes also remain weak, with changes in  $w$  no more than in the experiments where there is no wind feedback.

Northward Ekman velocities  $v$  out of the high-latitude Southern Ocean also remain nearly constant during  $FW_{SO}$  (figure not shown), changing by less than 5%. When repeating the experiments with the model’s wind feedback enabled, Ekman transport changes are

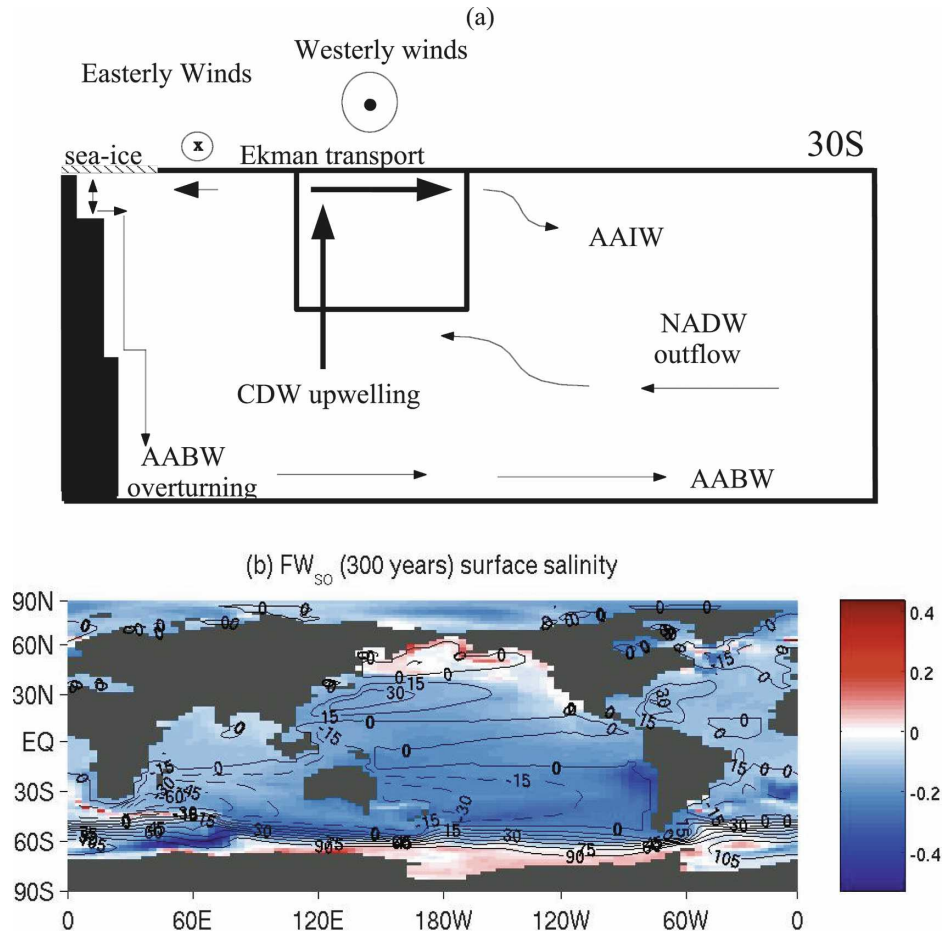


FIG. 6. (a) Schematic diagram showing the Southern Ocean thermohaline and wind-driven circulation described in the text. (b)  $FW_{SO}$  salinity difference from CNTRL at 300 yr with overlaid contours of ocean barotropic transport strength (Sv), showing a clear demarcation of the high-latitude enhanced salinity area. Contour interval is 15 Sv. All values are based on a 1-yr average.

at most 10%. Since the northward Ekman velocity remains similar but the transported water is much fresher, the net equivalent salt transport returning to the high-latitude Southern Ocean increases in response to the FW anomaly. This enables a mechanism for removing the added FW perturbation that is independent of AABW sinking.

To summarize, the flushing combination of wind-driven upwelling and meridional Ekman transport remains steady during  $FW_{SO}$ , removing added FW from the high-latitude Southern Ocean surface (as also seen by Stouffer et al. 2007) and providing a salt source to it, both of which are largely independent of the AABW sinking rate. Repeating these experiments with an ocean-atmosphere wind feedback enabled did not alter these results. Though this flushing is insufficient to maintain AABW sinking during the FW perturbation phase, once the FW addition has ceased, the surface

salinities return close to or even greater than those in CNTRL (Fig. 6b): The convection and overturning restart (Fig. 2). Figure 6b shows that by year 300, the added FW has been mostly dispersed to the north of the ACC, except in parts of the Weddell Sea and in the Indian Ocean sector of the Antarctic waters. A region of increased salinity in the high-latitude Southern Ocean is bordered to the north by the ACC. Since wind-driven upwelling is most efficient over the region of the ACC (Toggweiler et al. 2006), this further supports the significance of the winds in the reinitiation of AABW sinking. Finally, we further explored sensitivity experiments wherein the winds were shifted north by  $4^{\circ}$ – $6^{\circ}$  latitude (hence the upwelling of salty CDW is also shifted farther north). These experiments showed recovery of AABW after the FW pulse is terminated, only there is a slower recovery rate as the FW removal mechanism is less efficient.

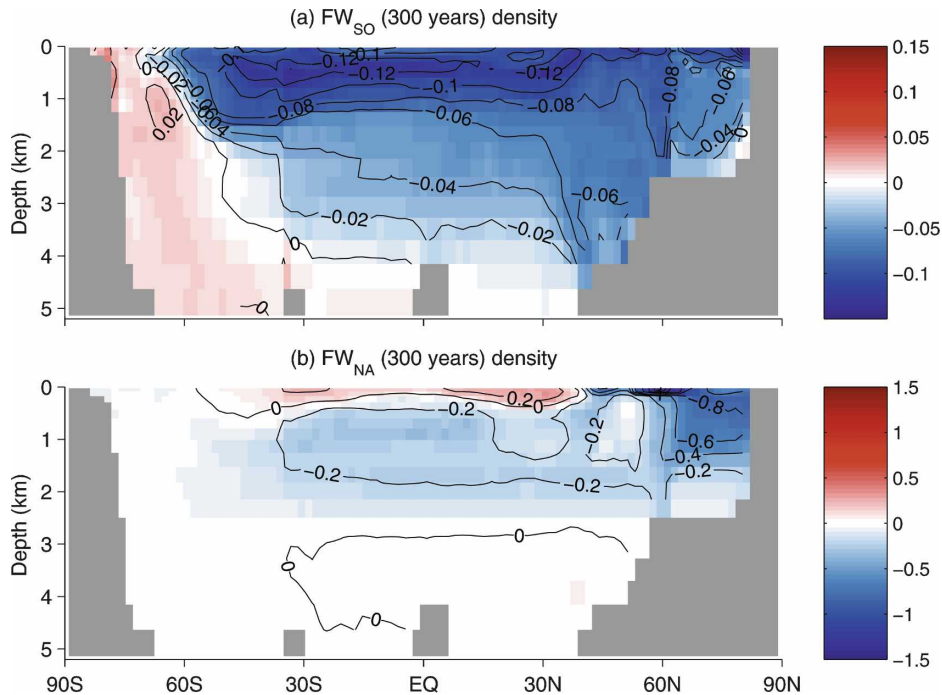


FIG. 7. Zonally averaged difference in density (from CNTRL) in  $FW_{SO}$  and  $FW_{NA}$  at the end of the FW pulse period (300 yr). The zonal average includes the Atlantic basin plus a circumpolar area in the Southern Hemisphere south of  $36.9^{\circ}S$ . The data are averaged for 1 yr at the end of the pulse period. The reference pressure is 2500 dbar. Note that the scale for  $FW_{SO}$  is a factor of 10 less than that for  $FW_{NA}$ . Contour interval: (a) 0.02 and (b)  $0.2 \text{ kg m}^{-3}$ .

In addition to the advective salt fluxes from vertical and horizontal ocean velocities, changes in surface processes also play a role in increasing the surface salinity once the FW pulse ends. At 150 yr in  $FW_{SO}$ , despite the constant surface dilution by the FW anomaly, surface salt fluxes over the Ross and Weddell Seas decrease less than over the other regions of the Southern Ocean. Figure 5b shows surface salt fluxes owing to evaporation, precipitation, and sea ice changes but not the FW addition term (the FW addition term is equivalent, at its maximum, to a salinity flux of  $1.9 \times 10^{-5} \text{ kg m}^{-2} \text{ s}^{-1}$  south of  $63^{\circ}S$ ). The areas of maximum Southern Ocean salt flux increase (Fig. 5b) correspond well to the maximum sea ice volume (height) increase in Fig. 5a. The enhanced ice production is due to surface cooling, which in turn is due to the suppression of the AABW overturn. This explains the more rapid return to AABW production in our study compared to Bi et al. (2001) who, by warming the globe as a whole, warmed the global ocean and reduced sea ice area, thus also reducing surface salt fluxes. Since in  $FW_{SO}$  this effect acts to increase AABW production after suppression by the FW anomaly, we can refer to it as a stabilizing (or negative) feedback. The sea ice feedback tends to work in the reverse, or positive, sense in the North

Atlantic where an increase in sea ice suppresses surface ocean heat loss/evaporation, thereby reducing deep overturning (see, e.g., Lohmann and Gerdes 1998). In this positive feedback scenario, sea ice acts to insulate the ocean from the colder overlying atmosphere. Unless there is sufficient sea ice transport away from the formation areas (achieved by the westerly winds in the Southern Hemisphere), sea ice will inhibit the heat exchange necessary for cooling of surface waters, and thus overturning. Clearly the North Atlantic and Antarctic regions differ in this regard.

In summary, once FW forcing ceases in  $FW_{SO}$ , localized convection is reestablished around Antarctica, aided by the perpetual upwelling of salty CDW combined with increased sea ice and a reduced stratification arising from deep ocean warming. The convection brings more warm, saline water to the surface (see Fig. 7a) that cools, sinks, and continues the process of reestablishing a density structure similar to the control experiment. A large reason for the differing THC responses between the hemispheres is the different way in which salt is transported poleward, which in turn is affected by different land mass geometries. The process of suppressing AABW with FW does not suppress the oceanic salt transport or fluxes that normally maintain

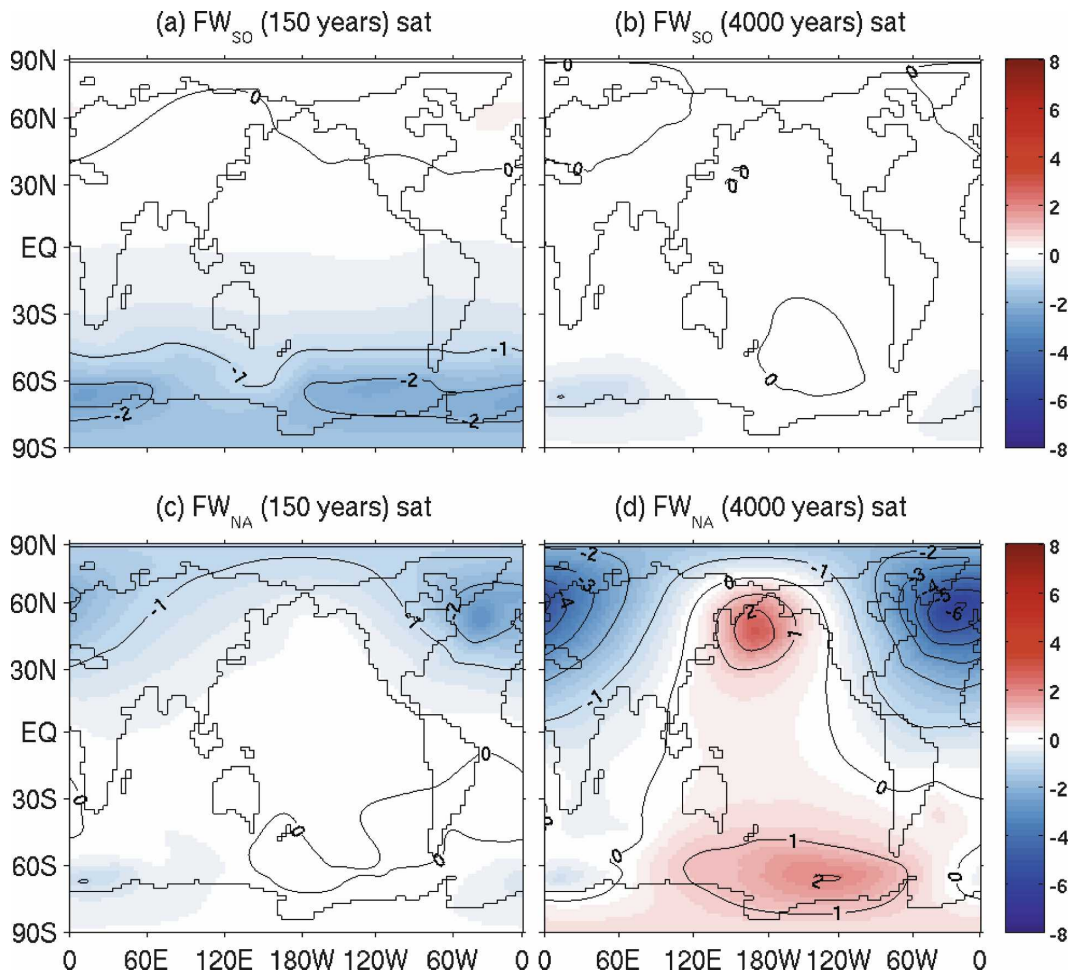


FIG. 8. Difference fields (from CNTRL) of surface sea and surface air temperature for  $FW_{SO}$  and  $FW_{NA}$  at (left) 150 yr and (right) 4000 yr. The data are taken from a 1-yr average. Contour interval:  $1^{\circ}\text{C}$ .

AABW production, quite unlike the classic Stommel (1961) climate response characteristic of the North Atlantic.

#### d. Climatic effects

The reduction in SST and surface atmospheric temperature (SAT) in  $FW_{SO}$  at 150 yr (Figs. 4c and 8a) is equivalent to a zonal average cooling of  $0.2^{\circ}$  and  $2.0^{\circ}\text{C}$ , respectively, south of  $63^{\circ}\text{S}$ . The maximum response in SAT is comparable to the corresponding year 150 zonal average cooling of SAT over the North Atlantic ( $2.1^{\circ}\text{C}$  north of  $51.3^{\circ}\text{N}$ ) in  $FW_{NA}$  (Fig. 8c). However, owing to the different long-term changes, the cooling over the North Atlantic increases to reach a steady-state value of  $4.5^{\circ}\text{C}$ , while the Southern Hemisphere SAT cooling is almost totally damped out within a few hundred years of the end of the FW pulse. The maximum zonal response in SST during  $FW_{SO}$  (at 150 yr) of  $0.2^{\circ}\text{C}$  is much

smaller than the  $1.4^{\circ}\text{C}$  seen over the North Atlantic in  $FW_{NA}$  at the same time (Fig. 4d). Like SAT, this SST cooling over the North Atlantic during  $FW_{NA}$  increases during the course of the experiment to reach a steady-state value of  $2.9^{\circ}\text{C}$  by year 4000, while in  $FW_{SO}$  it returns to within  $0.05^{\circ}\text{C}$  of CNTRL values a few hundred years after the FW pulse ends.

The maximum surface atmospheric cooling over the Australian and New Zealand region in  $FW_{SO}$  is almost  $1^{\circ}\text{C}$  (Fig. 8a), with the  $-2^{\circ}\text{C}$  contour almost reaching the southern tip of South America at 150 yr. The cooling over North America and Europe adjacent to the North Atlantic at the same time in  $FW_{NA}$  is of a similar order (Fig. 8c). However, this cooling increases over the course of the experiment to reach more than  $4^{\circ}\text{C}$  over parts of western Europe and eastern Canada (Fig. 8d), while the Southern Hemisphere cooling in  $FW_{SO}$  is almost totally removed by 4000 yr (Fig. 8b). Remnant cooling remains only near the Antarctic coastline and

this persists at less than  $1^{\circ}\text{C}$  cooling, giving a zonal average cooling of just  $0.3^{\circ}\text{C}$  south of  $63^{\circ}\text{S}$ .

Even though in  $\text{FW}_{\text{SO}}$  the maximum surface ocean temperature reduction over the Southern Ocean is modest, the temporary suppression of convection suppresses the upwelling of warmer water during the FW pulse period, allowing the sea ice volume to increase dramatically (Fig. 5a). The sea ice height over the major AABW formation regions of the Ross and Weddell Seas increases by up to 0.5 m, while the coverage area of sea ice also increases over other regions; both effects increase the original sea ice volume by more than 20%. A greater ocean surface area covered by sea ice leads to a reduction in heat fluxes from the ocean to the atmosphere, contributing significantly to the local cooling in atmospheric temperature. The sea surface temperature only cools slightly, because the high-latitude Southern Ocean is already close to the freezing point. Once the ocean comes back into equilibrium with the surface air temperature, ocean temperatures return to within  $0.05^{\circ}\text{C}$  of CNTRL by 4000 yr.

There is a “seesaw” response in  $\text{FW}_{\text{NA}}$  in which the South Pacific SAT increases in temperature by more than  $2^{\circ}\text{C}$  as less heat is transported into the North Atlantic and is eventually balanced by a heat gain in the south (Fig. 8d). Thus a NADW “shutdown” or weakening would possibly exacerbate the effects of global warming over this region of the Southern Hemisphere. In  $\text{FW}_{\text{SO}}$ , however, there is only a very weak interhemispheric response, with a slight temporary warming over the far North Atlantic (Fig. 8a).

Lower evaporation over the slightly cooler and ice-covered high-latitude Southern Ocean during AABW suppression results in a zonal average decrease in precipitation south of  $63^{\circ}\text{S}$  of around 10% ( $73 \text{ mm yr}^{-1}$ ), which could also aid in capping surface freshening (applied at the rate of  $600 \text{ mm yr}^{-1}$  at the height of the pulse). During peak FW addition, the ACC weakens by around 15 Sv (figure not shown) owing to the reduced meridional density gradient across the region.

#### e. Hysteresis experiments

In the hysteresis experiments we apply the FW flux at the rate of 0.2 Sv/1000 yr over the high-latitude Southern Ocean ( $\text{HYS}_{\text{SO}}$ ) and 0.08 Sv/1000 yr over the North Atlantic ( $\text{HYS}_{\text{NA}}$ ). The former is consistent with the North Atlantic hysteresis experiments carried out by Gregory et al. (2003). The initial  $\text{HYS}_{\text{SO}}$  experiment applied FW to the same limited area as the  $\text{FW}_{\text{SO}}$  experiments (south of  $63^{\circ}\text{S}$ ). However, in that experiment, after AABW initially showed a steady decrease, it rapidly reinitiated. Since FW does not accumulate at the Antarctic continental margin, the rate of FW addi-

tion becomes important: Surface and oceanic salt feedbacks in the Southern Ocean do not reinforce the applied freshening, as occurs in North Atlantic hysteresis experiments. Thus the AABW response to FW additions depends on the rate of change of the FW addition rate, not just the FW addition rate itself. To carry out the hysteresis experiments then, the area of the FW addition was extended north to  $60^{\circ}\text{S}$ , maintaining the same local FW fluxes, but increasing the net volume of water added. For  $\text{HYS}_{\text{SO}}$ , the linearly increasing FW flux was applied for 3500 yr before symmetrically returning to zero (Fig. 9b) at year 7000.

The hysteresis experiment  $\text{HYS}_{\text{SO}}$  results are shown in Fig. 9a (blue solid curve). It should be noted that, because of the dependence on the rate of change of FW addition rate, these curves are not unique. However, they do illustrate the entirely different behavior of AABW compared to the North Atlantic. Namely, because the feedbacks of the system do not reinforce the perturbation, the response of the overturning is not smooth. AABW rapidly switches back “on” in a series of steps a few hundred years after FW forcing reverses direction (at around 0.52 Sv). Though AABW seems to demonstrate two states for the same forcing at this time, these are not steady as revealed by forward integration with FW forcing held constant (figure not shown). AABW switches on more quickly in the downward phase of the FW application. In these hysteresis experiments, with salt compensation over the World Ocean outside of Antarctica (including the North Atlantic), NADW starts to decrease a few hundred years after the Southern Ocean FW flux has started to decrease (increase over the North Atlantic). To reduce this complicating feature of a reacting NADW water mass, an experiment with no salt compensation is also shown (blue dashed line). AABW recovers along nearly the same path on reversal of the FW forcing, until a large oscillation occurs toward the end of the experiment. The oscillations seen in the last few centuries of these experiments are due to extremely reduced stratification in a much fresher ocean, making vigorous overturning more susceptible to surface heat and salinity flux changes.

## 4. Summary and conclusions

We have demonstrated that the difference in response to FW perturbations of the North Atlantic and high-latitude Southern Ocean arises from different thermal and salt feedbacks, caused by fundamental differences in land mass geometries. In the North Atlantic, the dominant salt feedback is via surface water advection from lower latitudes. If NADW slows, this salt

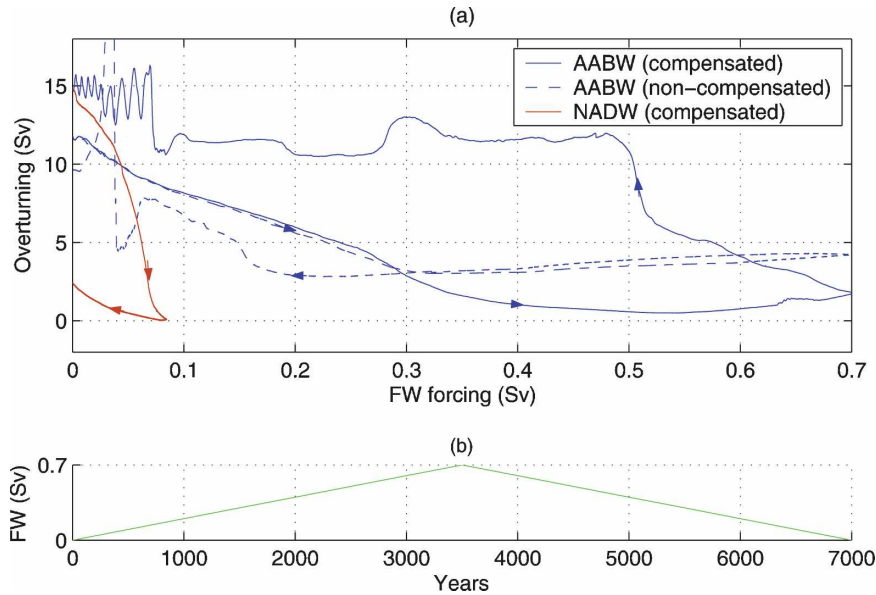


FIG. 9. Overturning response to a slow FW forcing [ $0.2 \text{ Sv} (1000 \text{ yr})^{-1}$  for  $\text{HYS}_{\text{SO}}$ , and  $0.08 \text{ Sv} (1000 \text{ yr})^{-1}$  for  $\text{HYS}_{\text{NA}}$ ]. (a) Overturning vs FW forcing. The trajectories show FW forcing increasing to the right and decreasing to the left. The North Atlantic overturning (blue line) can be considered to be in quasi steady state at each point along the curve. The Southern Ocean overturning for different FW forcings is not in quasi steady state: onward integration with forcing held constant does not maintain the same state. (b) The FW forcing vs time. Vertical scale is in Sv.

advection also slows, and the natural feedbacks of the system enhance the applied perturbation (Fig. 10). The presence of the Drake Passage gap blocks this feedback in the Southern Hemisphere, and, instead, it is the up-

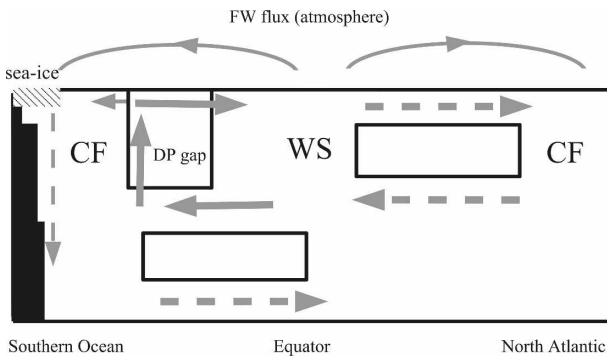


FIG. 10. Schematic diagram highlighting the key salinity feedbacks in the high-latitude (left) Southern Ocean and (right) North Atlantic based on the simplified Stommel (1961) box model, where sinking occurs in the high-latitude basin in each case. WS denotes warm, saline; CF denotes cold, fresh; and DP gap denotes Drake Passage. Arrows indicate salt transport mechanisms. A dashed line indicates that the transport is dependent on sinking (in either hemisphere). A solid line indicates that the transport is independent of sinking. In the North Atlantic, there is one positive (destabilizing) feedback. In the high-latitude Southern Ocean, there is one independent feedback (wind-driven upwelling) and one stabilizing feedback (sea ice). Thermal feedbacks are not shown.

welling of saline CDW and northward Ekman transport of FW that transports salt into the high-latitude Southern Ocean (Fig. 10). Critically, the upwelling of deep saline water and northward Ekman transport of FW is largely independent of the rate of AABW sinking. Thus, when bottom-water sinking is suppressed, salt continues to accumulate below the surface FW lens. Eventually, once the surface waters cool and the FW lens is dispersed, AABW formation is readily reestablished. The system was found to be incapable of maintaining FW anomalies at the high-latitude Southern Ocean surface in the absence of sustained forcing. Sea ice is affected by FW addition but, in a stabilizing sense, namely, on suppression of AABW, there is surface cooling, growth of more sea ice, and hence an increase in surface brine input. Combined with a deep ocean warming while AABW slows, these effects lead to gravitational instability and the reestablishment of convection, bringing deep saline water to the surface where the thin FW layer is further mixed away. Overturning is thus restarted soon after the FW perturbation has ceased.

The difference in North Atlantic and Antarctic salt feedbacks is due to 1) colder Antarctic waters that allow for extensive sea ice formation once overturning is slowed; 2) differing continental geometries that allow wind-forced upwelling to dominate in the Southern

Ocean; and 3) a different vertical ocean structure with warm deep water underlying cold surface water in the high-latitude Southern Ocean. If we accept that the cooler temperatures around Antarctica are due, at least in part, to the thermal isolation caused by this differing continental geometry and that the persistence of the wind-forced upwelling arises because of the Drake Passage effect, then we conclude that the differing land mass geometry is the fundamental reason for the difference in behavior of NADW and AABW under identical FW perturbations.

It is interesting to note the remarkable steadiness of the high-latitude Southern Ocean temperature over the course of FW<sub>SO</sub> (maximum zonal mean change, south of 63°S, of 0.2°C from section 3d). Ocean temperatures in this region are kept so cold (near freezing point) by subzero katabatic winds blowing over the ocean, originating over the Antarctic land-ice mass. In the model, the effect of the Antarctic ice on maintaining cool SST is parameterized by way of meridional atmospheric diffusion. This influence of the land ice maintains colder surface temperatures than would otherwise be expected, even when the higher-latitude regions of the AABW formation zones (compared to the North Atlantic) are taken into account. In fact, this thermal discrepancy between the Southern and Northern Hemisphere overturning regions leads to water densities in the polar Southern Ocean that are greater than any other water mass in the global ocean. The large density difference between NADW and AABW (0.5 kg m<sup>-3</sup>), combined with the deep Drake Passage sill, leads to AABW being highly stable to FW perturbations. This leaves AAIW and NADW as the main interactors in an interhemispheric seesaw of the ocean THC. If the Antarctic terrestrial ice sheet were absent or the FW forcing persisted on time scales that allowed the ice sheet to adapt, then the surface water would be warmer and the stability of AABW is likely to be reduced.

In conclusion, the response of AABW to FW perturbations is entirely different compared to NADW. In the North Atlantic, the freshening is enhanced by a positive salt advection feedback. In the Southern Ocean, the salt feedbacks are stabilizing and combine to restart AABW after the FW addition ceases, regardless of the FW flux intensity or duration. This allows the thermal preference for Antarctic sinking to preclude a steady off state for AABW in the model considered here. Although these experiments have been conducted using a simple atmospheric model rather than a 3D dynamic AGCM, the stabilizing feedbacks that have been highlighted are mainly limited to the ocean-ice system. In addition, all experiments have been rerun with a dynamic wind feedback included and robust results were

obtained. Hence, it is most likely that the feedbacks identified in this study would be present in full dynamics coupled climate system models.

*Acknowledgments.* R. J. Stouffer and three anonymous reviewers provided useful feedback on the original manuscript. This research is supported by the Australian Research Council and Australia's Antarctic Science Program.

#### REFERENCES

- Bates, M. L., M. H. England, and W. P. Sijp, 2005: On the multi-century Southern Hemisphere response to changes in atmospheric CO<sub>2</sub> concentration in a Global Climate Model. *Meteor. Atmos. Phys.*, **89**, 17–36.
- Bi, D., W. F. Budd, A. C. Hirst, and X. Wu, 2001: Collapse and reorganisation of the Southern Ocean overturning under global warming in a coupled model. *Geophys. Res. Lett.*, **28**, 3927–3930.
- Bitz, C. M., and W. H. Lipscomb, 1999: An energy-conserving thermodynamic model of sea ice. *J. Geophys. Res.*, **104**, 15 669–15 677.
- Brix, H., and R. Gerdes, 2003: North Atlantic Deep Water and Antarctic Bottom Water: Their interaction and influence on the variability of the global ocean circulation. *J. Geophys. Res.*, **108**, 3022, doi:10.1029/2002JC001335.
- Bryan, F., 1986: High-latitude salinity effects and interhemispheric thermohaline circulations. *Nature*, **323**, 301–304.
- Bryan, K., and L. J. Lewis, 1979: A water mass model of the world ocean. *J. Geophys. Res.*, **84**, 2503–2517.
- Clark, P. U., N. G. Pisias, T. F. Stocker, and A. J. Weaver, 2002: The role of the thermohaline circulation in abrupt climate change. *Nature*, **415**, 863–869.
- Duffy, P. B., and K. Caldeira, 1997: Sensitivity of simulated salinity in a three-dimensional ocean model to upper ocean transport of salt from sea-ice formation. *Geophys. Res. Lett.*, **24**, 1323–1326.
- Gent, P. R., and J. C. McWilliams, 1990: Isopycnal mixing in ocean circulation models. *J. Phys. Oceanogr.*, **20**, 150–155.
- Gill, A. E., 1982: *Atmosphere–Ocean Dynamics*. Academic Press, 662 pp.
- Goodman, J. P., 1998: The role of North Atlantic Deep Water formation in an OGCM's ventilation and thermohaline circulation. *J. Phys. Oceanogr.*, **28**, 1759–1785.
- Gregory, J. M., O. A. Saenko, and A. J. Weaver, 2003: The role of the Atlantic freshwater balance in the hysteresis of the meridional overturning circulation. *Climate Dyn.*, **21**, 707–717.
- Kalnay, E., and Coauthors, 1996: The NCEP–NCAR 40-Year Reanalysis Project. *Bull. Amer. Meteor. Soc.*, **77**, 437–471.
- Keeling, R. F., and B. B. Stephens, 2001: Antarctic sea ice and the control of Pleistocene climate instability. *Paleoceanography*, **16**, 112–131.
- Levitus, S., and T. P. Boyer, 1994: *Temperature*. Vol. 4, *World Ocean Atlas 1994*, NOAA Atlas NESDIS 4, 117 pp.
- , R. Burgett, and T. P. Boyer, 1994: *Salinity*. Vol. 3, *World Ocean Atlas 1994*, NOAA Atlas NESDIS 3, 99 pp.
- Lohmann, G., and R. Gerdes, 1998: Sea ice effects on the sensitivity of the thermohaline circulation. *J. Climate*, **11**, 2789–2803.

- Manabe, S., and R. J. Stouffer, 1988: Two stable equilibria of a coupled ocean–atmosphere model. *J. Climate*, **1**, 841–866.
- Orsi, A. H., G. C. Johnson, and J. L. Bullister, 1999: Circulation, mixing and production of Antarctic Bottom Water. *Prog. Oceanogr.*, **43**, 55–109.
- , S. S. Jacobs, A. L. Gordon, and M. Visbeck, 2001: Cooling and ventilating the abyssal ocean. *Geophys. Res. Lett.*, **28**, 2923–2926.
- Pacanowski, R., 1995: MOM 2 documentation, user’s guide and reference manual. NOAA GFDL Ocean Group Tech. Rep. 3, 232 pp.
- Prange, M., V. Romanova, and G. Lohmann, 2002: The glacial thermohaline circulation: Stable or unstable? *Geophys. Res. Lett.*, **29**, 2028, doi:10.1029/2002GL015337.
- Rahmstorf, S., 1993: A fast and complete convection scheme for ocean models. *Ocean Modell.*, **101**, 9–11.
- , 1996: On the freshwater forcing and transport of the Atlantic thermohaline circulation. *Climate Dyn.*, **12**, 799–811.
- , and M. H. England, 1997: Influence of Southern Hemisphere winds on North Atlantic Deep Water flow. *J. Phys. Oceanogr.*, **27**, 2040–2054.
- , and Coauthors, 2005: Thermohaline circulation hysteresis: A model intercomparison. *Geophys. Res. Lett.*, **32**, L23605, doi:10.1029/2005GL023655.
- Saenko, O. A., and A. J. Weaver, 2001: Importance of wind-driven sea ice motion for the formation of Antarctic Intermediate Water in a Global Climate Model. *Geophys. Res. Lett.*, **28**, 4147–4150.
- , J. M. Gregory, A. J. Weaver, and M. Eby, 2002: Distinguishing the influence of heat, freshwater, and momentum fluxes on ocean circulation and climate. *J. Climate*, **15**, 3686–3697.
- , A. J. Weaver, and J. M. Gregory, 2003: On the link between the two modes of the ocean thermohaline circulation and the formation of global-scale water masses. *J. Climate*, **16**, 2797–2801.
- , A. Schmittner, and A. J. Weaver, 2004: The Atlantic–Pacific seesaw. *J. Climate*, **17**, 2033–2038.
- Sen Gupta, A., and M. H. England, 2007: Coupled ocean–atmosphere feedback in the Southern Annular Mode. *J. Climate*, **20**, 3677–3692.
- Sijp, W. P., and M. H. England, 2005: Role of the Drake Passage in controlling the stability of the ocean’s thermohaline circulation. *J. Climate*, **18**, 1957–1966.
- , and —, 2006: Sensitivity of the Atlantic thermohaline circulation and its stability to basin-scale variations in vertical mixing. *J. Climate*, **19**, 5467–5478.
- Stommel, H., 1961: Thermohaline convection with two stable regimes of flow. *Tellus*, **13**, 224–230.
- Stouffer, R. J., and S. Manabe, 2003: Equilibrium response of thermohaline circulation to large changes in atmospheric CO<sub>2</sub> concentration. *Climate Dyn.*, **20**, 759–773.
- , D. Seidov, and B. Haupt, 2007: Climate response to external sources of freshwater: North Atlantic versus the Southern Ocean. *J. Climate*, **20**, 436–448.
- Talley, L. D., J. L. Reid, and P. E. Robbins, 2003: Data-based meridional overturning streamfunctions for the global ocean. *J. Climate*, **16**, 3213–3226.
- Toggweiler, J. R., and B. L. Samuels, 1993: New radiocarbon constraints on the upwelling of abyssal water in the ocean’s surface. *The Global Carbon Cycle*, M. Heimann, Ed., Springer-Verlag, 333–366.
- , and —, 1995: Effect of Drake Passage on the global thermohaline circulation. *Deep-Sea Res. I*, **42**, 477–500.
- , J. L. Russell, and S. R. Carson, 2006: Midlatitude westerlies, atmospheric CO<sub>2</sub>, and climate change during the ice ages. *Paleoceanography*, **21**, PA2005, doi:10.1029/2005PA001154.
- Vellinga, M., and R. A. Wood, 2002: Global climatic impacts of a collapse of the Atlantic thermohaline circulation. *Climatic Change*, **54**, 251–267.
- Weaver, A. J., and Coauthors, 2001: The UVic Earth System Climate Model: Model description, climatology, and applications to past, present, and future climates. *Atmos.–Ocean*, **39**, 1067–1109.
- Yin, J., M. E. Schlesinger, N. G. Andronova, S. Malyshev, and B. Li, 2006: Is a shutdown of the thermohaline circulation irreversible? *J. Geophys. Res.*, **111**, D12104, doi:10.1029/2005JD006562.